Available online at website: https://journal.bcrec.id/index.php/bcrec

Bulletin of Chemical Reaction Engineering & Catalysis, 21 (1) 2026, 112-127

Original Research Article

Influence of Nickel and Aluminum in Bentonite for Ethanol-to-Gasoline Reaction

Robert R. Widjaya[1*], Yusraini D. I. Siregar[3], Syifa H. Nabillah[3], Nino Rinaldi[1], Sabar P. Simanungkalit[1], Joni Prasetyo[2], Adid A. Dwiatmoko[1]

[1]Research Center for Catalysis, National Research and Innovation Agency, KST. BJ. Habibie PUSPIPTEK Serpong, Tangerang Selatan, Indonesia.
[2]Research Center for Molecular Chemistry, National Research and Innovation Agency, KST. BJ. Habibie PUSPIPTEK Serpong, Tangerang Selatan, Indonesia.
[3]Department of Chemistry, UIN Syarif Hidayatullah Jakarta, Indonesia.

Received: 29th September 2025; Revised: 10th December 2025; Accepted: 11th December 2025
Available online: 12th January 2026; Published regularly: April 2026

Abstract

Bentonite can be used as a catalyst due to its flexible structure. However, it has several drawbacks, including low thermal and hydrothermal stability, as well as a small surface area and pore volume. This study aims to modify the structure of bentonite using the pillared clay (PILC) method, in order to improve its physicochemical properties and catalytic activity. The bentonite was pillared with aluminium (Al/PILC), nickel (Ni/PILC), and a combination of both metals (Al-Ni/PILC). Catalyst characterization was carried out using X-Ray Diffraction (XRD), X-Ray Fluorescence (XRF), Surface Area Analyzer (SAA), Fourier Transform Infrared Spectroscopy (FTIR), Temperature Programmed Desorption of Ammonia (TPD-NH_3), Thermogravimetric Analysis-Differential Scanning Calorimetry (TGA-DSC), and Gas Chromatography with Flame Ionization Detection (GC-FID). XRD analysis showed an increase in the interlayer spacing, the largest basal spacing is observed in Al/PILC. XRF results indicated an increase in the composition of Al_2O_3 and NiO in all four catalysts. SAA analysis demonstrated an increase in surface area and pore volume across the catalysts, the highest surface area is exhibited by Al/PILC (187.83 m^2/g), while the largest pore diameter is observed in Al-Ni/PILC (12.83 nm). The acidity analysis using TPD-NH_3 shows that Al/PILC possesses the highest acidity value of 2.34 mmol/g. The presence of Brønsted acid sites was confirmed through FTIR analysis. TGA-DSC analysis indicated an improvement in the thermal stability of all tested catalysts. The Al/PILC catalyst showed the best performance at 150 °C. When the reaction temperature was increased to 250 °C, the Al-Ni/PILC catalyst demonstrated the highest efficiency in the ethanol-to-gasoline conversion process.

Keywords: Bentonite; Al-Ni/PILC; Aluminium; Nickel; Gasoline

How to Cite: Widjaya, R. R., Siregar, Y. D. I., Nabillah, S. H., Rinaldi, N., Simanungkalit, S. P., Prasetyo, J., Dwiatmoko, A. (2026). Influence of Nickel and Aluminum in Bentonite for Ethanol-to-Gasoline Reaction. *Bulletin of Chemical Reaction Engineering & Catalysis*, 21 (1), 112-127. (doi: 10.9767/bcrec.20502)

Permalink/DOI: https://doi.org/10.9767/bcrec.20502

1. Introduction

For over three centuries, fossil fuels have served as the principal raw material in conventional petroleum production [1]. However, according to the International Energy Agency (IEA) [2], the depletion of fossil fuel reserves and their declining availability are expected to render global dependence on fossil fuels unsustainable in the near future. Consequently, the pursuit of renewable and alternative energy sources has become an urgent priority to ensure long-term energy security and environmental sustainability. Catalysis plays a vital role in the production of alternative fuels, frequently involving catalytic processes facilitated by clay-based catalysts [3].

Among various renewable options, bioethanol has emerged as a promising feedstock due to its renewability, abundance, and potential to be produced from biomass or agricultural waste.

* Corresponding Author.
Email: robe007@brin.go.id (R.R. Widjaya)

Traditionally, bioethanol is used as a gasoline additive or blending component; however, it can also serve directly as a feedstock in the ethanol-to-gasoline (ETG) process, a catalytic pathway that converts ethanol into hydrocarbons equivalent to conventional gasoline [19]. This process is advantageous because it can utilize ethanol, water mixtures with concentrations below 60%, typical of bioethanol fermentation, without requiring additional purification steps such as distillation or membrane separation [20]. Hence, ETG catalysis provides an efficient and economically viable approach for producing drop-in biofuels compatible with existing energy infrastructures.

The success of the ETG process depends critically on the catalyst employed, as the structural and acidic properties of catalysts determine both activity and selectivity. In this regard, clay-based catalysts such as bentonite have attracted considerable attention owing to their natural abundance, high surface area, ion exchange capacity, adjustable acidity, and good thermal stability. Bentonite, belonging to the smectite mineral group, possesses a layered crystalline structure with interlayer spaces that can be modified to enhance porosity and catalytic performance. Its swelling and adsorption characteristics enable transformation of the pore system from microporous to mesoporous, thus improving accessibility of reactants to active sites.

According to Li *et al.* [4], aluminum oxide exhibits acidic properties and possesses a high surface area, making it an excellent support material for metal-based catalysts such as platinum, palladium, or other transition metals. In this context, aluminum contributes to enhancing both the activity and selectivity of the catalyst. According to Shi *et al.* [5], nickel plays a crucial role in hydrogenation, dehydrogenation, and hydrocarbon conversion catalysis. The advantages of nickel as a catalyst include its high catalytic activity, stability, and relatively low cost. Nickel-based catalysts have been widely applied in chemical production, fuel processing, and the petrochemical industry.

Although a catalyst may exhibit strong acidity that enhances its initial activity, it often suffers from a decline in performance over time during cracking reactions due to the accumulation of carbon deposits that block active sites, a phenomenon known as catalyst deactivation [6]. This issue can be mitigated by impregnating transition metals onto the catalyst support. These metals facilitate hydrogenation through the homolytic dissociation of hydrogen molecules, thereby suppressing carbon residue formation and enhancing the catalyst's activity, selectivity, and stability [7]. Nickel is commonly employed alongside noble metals such as palladium in various catalytic systems to improve performance [8]. When nickel is impregnated into bentonite clay, it demonstrates promising catalytic activity in hydrogenation. Furthermore, incorporation of nickel into zeolite materials can significant increase the catalyst's acidity by up to 2.12 times compared to its original state [9,10]. In hydrocracking studies of ethanol using a Al/Ni catalyst, it was found that increasing the nickel concentration improved the yield of liquid products, with gasoline being the predominant fraction obtained [11].

Ethanol is an alcohol compound with the chemical formula C_2H_5OH and a boiling point of 78.4 °C. Its molecular structure consists of a two-carbon chain bonded to a hydroxyl (OH) group, the presence of which imparts polarity to the ethanol molecule. This polarity enables ethanol to dissolve in water and function as an effective solvent. Additionally, ethanol can form hydrogen bonds with water molecules, resulting in significant intermolecular interactions [13].

Recently, bentonite has emerged as the predominant type of clay used in catalytic applications. Bentonite exhibits distinctive properties, including a high specific surface area due to its small particle size, adjustable acidity, ion exchange capacity [12], as well as binding and swelling abilities that enable selective adsorption of molecules. Bentonite possesses an inherent swelling capacity that enables the modification of its pore structure into microporous or mesoporous forms, enhancing its suitability as a catalyst. The stabilization of shale swelling caused by hydration can be achieved through two primary methods: (i) intercalation of small organic molecules into the interlayer spaces of the shale, and (ii) incorporation of high molecular weight polymers within the shale matrix [14,15]. An effective technique for tailoring pore size, thereby improving catalytic activity and thermal stability, is the pillaring of bentonite with metal oxides or metal species [16,17]. This method involves the intercalation of large inorganic polyhydroxocation species such as Al, Zr, Ti, Fe, or Cr (either individually or in combination with other cations) into the clay interlayers, followed by thermal treatment typically in the range of 300–700 °C. As metals and their oxides can function as catalysts, their incorporation into bentonite results in composites with enhanced functional groups and increased surface active sites [17]. Metal oxides thus play a dual role in bentonite modification, serving both as pillaring agents and catalytic components. Common metal oxides used for this purpose include Al_2O_3, ZrO_2, TiO_2, Fe_2O_3, and Cr_2O_3 [11–17].

Gasoline, commonly referred to as petrol, is a liquid mixture of straight-chain hydrocarbons ranging from C_5 (pentane) to C_{12} (dodecane), exhibiting boiling points between 50 and 200 °C. It is predominantly utilized as a fuel for internal

combustion engines in motor vehicles and various other mechanical apparatuses. According to Leffler *et al.* [18] finding, gasoline comprises a complex mixture of hydrocarbons derived from the fractional distillation of crude oil during the refining process. Typically, gasoline contains compounds such as heptane, octane, and other light hydrocarbons. The heterogeneity of these components confers the physicochemical properties necessary to optimize combustion efficiency in internal combustion engines.

In the ethanol-to-gasoline (ETG) process, catalyst specifications must be tailored to optimize key properties that enhance catalytic activity and, consequently, catalyst selectivity [21]. Therefore, modifications to the interlayer spacing and the bentonite surface, which acts as a catalyst support, can be implemented to optimize the catalytic process. These modifications aim to increase acidity, improve water resistance, and enhance pore volume, surface area, and thermal stability (above 400 °C) [22,23].

A method to modify bentonite as an ETG catalyst involves pillarization (Pillared Interlayer Clay or PILC). The formation of oxide pillars as active components significantly influences the surface properties of bentonite. Thus, pillarization optimizes the ratio of Lewis to Brønsted acid sites [24]. Although a catalyst may exhibit strong acidity resulting in high activity, it often fails to maintain long-term catalytic performance in ETG reactions due to the formation of residues that block active sites, leading to catalyst deactivation. This issue can be addressed by combining pillarization with transition metal on the catalyst support. Therefore, this study aims to investigate the influence of nickel and aluminum modification in bentonite on its catalytic performance in the ethanol-to-gasoline (ETG) reaction, focusing on the improvement of catalyst acidity, stability, and product selectivity. Thereby contributing to the development of efficient, stable, and sustainable clay-based catalysts for alternative fuel production.

2. Materials and Methods

2.1. Preparation Materials

Bentonite was prepared using a commercial bentonite product (Sigma-Aldrich, catalog number 285234). Aluminum chloride hexahydrate ($AlCl_3.6H_2O$), Nickel(II) Chloride hexahydrate (NiCl2.6H2O) from Merck (1.06717.0250), sodium hydroxide (NaOH), and silver nitrate ($AgNO_3$, 0.1 M) were purchased from Merck. Ethanol (99.5% purity) was obtained from Smart Lab (product code A-1035). Distilled water and hydrogen gas (H_2) were also used in the synthesis process. A metal alloy-modified bentonite was synthesized using the pillaring method. The degree of hydrolysis, defined as the ratio of OH^- ions to moles of pillar metal, was maintained at 2. The concentrations of the pillar metal solution and the NaOH solution were 0.1 M.

2.2. Preparation of Aluminum Polycation Solution

A total of 12.07 g of $AlCl_3.6H_2O$ powder was dissolved in 500 mL of distilled water in a 1 L beaker, with continuous stirring using a magnetic stirrer on a hotplate for 2 hours. In a separate beaker, 4 g of solid NaOH was dissolved in 500 mL of distilled water under the same stirring conditions. The resulting NaOH solution was then added to the aluminum solution using a peristaltic pump at a flow rate of 0.56 mL/min, while vigorous stirring was maintained for 12 hours at room temperature. This process resulted in the formation of an aluminum polycation solution.

2.3. Preparation of Nickel Polycation Solution

A variation in the preparation of nickel polycation solutions was performed using molar ratios of 5 and 10. Specifically, 5.94 g (for the 5:1 ratio) and 11.89 g (for the 10:1 ratio) of $NiCl_2.6H_2O$ powder were each dissolved in 500 mL of distilled water in separate 1 L beakers, with continuous stirring using a magnetic stirrer on a hotplate for 2 hours. In a separate beaker, 4 g of solid NaOH was dissolved in 500 mL of distilled water under the same stirring conditions. The prepared NaOH solution was then added to the nickel solution using a peristaltic pump at a flow rate of 0.56 mL/min, while vigorous stirring was maintained for 12 hours at room temperature. This process resulted in the formation of a nickel polycation solution.

2.4. Pillarization of Bentonite with Aluminum and Nickel Polycation Solutions

A total of 5 g of bentonite was dispersed in 500 mL of distilled water, then heated at a constant temperature of 60 °C while stirring with a magnetic stirrer for 2 hours until a bentonite suspension was formed. Each of the 500 mL aluminum polycation solution and 500 mL nickel polycation solution was slowly added to the bentonite suspension under continuous stirring into separate glass beakers. The mixture was then stirred for an additional 24 hours at room temperature. Subsequently, a chloride (Cl^-) test was performed using $AgNO_3$, if a white precipitate was still observed, the mixture was washed with distilled water until no precipitate formed. The resulting Al/PILC and Ni/PILC suspensions were centrifuged at 5500 rpm for 5 minutes at 27 °C. The obtained precipitates were dried in an oven at 80 °C for 24 hours to yield the Al/PILC and Ni/PILC catalysts. These catalysts were then calcined in a furnace at 400 °C for 4 hours. The final catalysts were weighed and stored in sealed vials.

2.5. Pillarization of Bentonite with Al-Ni Polycation Solution

A volume of 500 mL of distilled water was placed into each of three separate glass beakers. Subsequently, 12.07 g of $AlCl_3.6H_2O$ was added to the first beaker, 11.89 g of $NiCl_2.6H_2O$ was added to the second beaker, and 4 g of NaOH pellets was added to the third beaker. Each solution was stirred with a magnetic stirrer for 2 hours. The nickel solution was then added to the aluminum solution and stirred for an additional 2 hours. Finally, the prepared NaOH solution was added to the combined Al-Ni solution using a peristaltic pump at a flow rate of 0.56 mL/min, while vigorous stirring was maintained for 12 hours at room temperature until an Al-Ni polycation solution was formed.

The prepared Al-Ni polycation solution was slowly added to a 1% bentonite suspension under continuous stirring. The mixture was then stirred for an additional 24 hours at room temperature. Subsequently, a chloride (Cl^-) test was performed using $AgNO_3$, if a white precipitate was still observed, the suspension was washed with distilled water until no precipitate remained. The resulting Al-Ni/PILC suspension was centrifuged at 5500 rpm for 5 minutes at 27 °C. The obtained precipitate was collected and dried in an oven at 80 °C for 24 hours to yield the Al-Ni/PILC catalyst, which was then calcined in a furnace at 400 °C for 4 hours. The final catalyst was weighed and stored in sealed vials.

2.6. Catalyst Characterizations

The catalyst material was characterized using a range of analytical techniques. X-ray diffraction (XRD) analysis was performed using a Panalytical Varian AERIS diffractometer with Cu-Kα radiation (λ = 1.54 Å), operated at 40 kV and 15 mA, and a scan rate of 2 °/min. This analysis was conducted to determine the interlayer spacing (d_{001}) and the crystallinity of the material, enabling the identification of crystalline phases present in the catalyst. The distribution of metal oxides within the interlayer and on the bentonite surface was analyzed by X-ray fluorescence (XRF) spectroscopy using a Bruker S2 PUMA instrument under a helium gas flow. Functional groups and surface acidity were identified using Fourier Transform Infrared Spectroscopy (FTIR) with a Bruker Tensor II system, employing the KBr pellet method and Prestige-21 with ATR 4000, connected to an automated data acquisition system. Acidity was further analyzed via temperature-programmed desorption of ammonia (TPD-NH_3) using a Micromeritics Chemisorb 2750 instrument. Samples were pretreated at 350 °C for 60 minutes under helium flow, followed by ammonia adsorption and desorption steps. Thermogravimetric analysis (TGA) was performed using a LINSEIS L70/2171 instrument by heating the samples from 300 °C to 1000 °C at a rate of 10 °C/min under a nitrogen atmosphere. Surface area and porosity were measured using a Micromeritics TriStar II 3020 surface area analyzer, based on the Brunauer–Emmett–Teller (BET) method with nitrogen adsorption. The analysis used a 10-second equilibration interval, a sample mass of 0.35 g, a cold free space volume of 32.81 cm^3, and a sample density of 1 g/cm^3. The Barrett–Joyner–Halenda (BJH) method was applied to determine pore size distribution and specific surface area.

2.7. Catalyst Testing

In this study, various catalysts bentonite, Al/bentonite, Ni/bentonite, and Al-Ni/bentonite were employed for the catalytic conversion of ethanol to biogasoline in a batch-scale autoclave reactor. The catalyst was used at a ratio of 0.5 g per 10 mL of ethanol (equivalent to a 1:20 w/v ratio) in the reactor. Hydrogen gas was introduced into the reactor (Figure 1), purged three times, and maintained at a pressure of 1 atm during the reaction. The reaction was carried out at 150 °C for 3 hours with stirring at 200 rpm. Following the reaction, the product mixture was filtered through Whatman paper, and the liquid phase was collected for analysis. The product composition was analyzed using Gas Chromatography with a Flame Ionization Detector (GC-FID), utilizing an Agilent 113-2032 Carbowax/20M column (30 m × 320 µm, 25 µm) coupled with the FID detector.

Conversion refers to the fraction (or percentage) of a reactant that has been transformed into products during a catalytic reaction. It indicates how effectively the catalyst promotes the reaction of the feedstock. In this study, catalyst performance in the ethanol-to-gasoline (ETG) reaction was evaluated in terms of conversion and selectivity. All catalytic reactions were conducted under steady-state conditions, and the outlet composition was

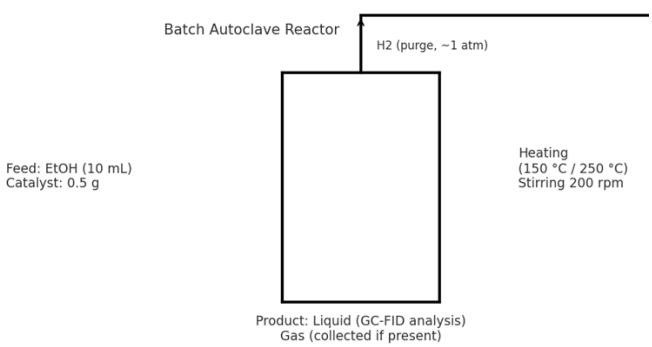

Figure 1. A schematic diagram of the reactor and testing setup.

analyzed using gas chromatography (GC–FID). Quantification of reactant and product concentrations was achieved by integrating the chromatographic peak areas and converting them to molar quantities using calibration curves derived from standard compounds.

Reactant Conversion represents the fraction of the feedstock that undergoes chemical transformation during the catalytic reaction. In this study, the conversion of ethanol (X_{ethanol}) was determined according to the following equation:

$$X_{\text{ethanol}}(\%) = \frac{F_{\text{in, ethanol}} - F_{\text{out, ethanol}}}{F_{\text{in, ethanol}}} \times 100 \quad (1)$$

where $F_{\text{in, ethanol}}$ and $F_{\text{out, ethanol}}$(mol.s^{-1}) denote the molar flow rates of ethanol at the reactor inlet and outlet, respectively. The molar flow rates were calculated based on GC-determined concentrations, assuming ideal gas behavior under reaction conditions. This parameter indicates the catalytic activity of the material toward ethanol conversion.

Selectivity reflects the proportion of a specific product formed relative to the total amount of products generated, thereby illustrating the capability of the catalyst to direct the reaction pathway toward the desired product. The selectivity of product i (S_i) was calculated as follows:

$$S_i(\%) = \frac{n_i}{\sum n_j} \times 100 \quad (2)$$

where n_i (mol) represents the number of moles of product i (e.g., gasoline-range hydrocarbons), and $\sum n_j$corresponds to the total moles of all products formed. In this work, hydrocarbons within the C_5–C_{12} range were classified as the gasoline fraction.

3. Results and Discussion

3.1. XRD Analysis

The low-angle XRD pattern in Figure 2 shows that the d001 reflection peak of bentonite before pillaring was detected at a 2θ angle of 6.34°, corresponding to a basal spacing of 13.93 Å. This observation is consistent with a previous study by Widjaya *et al.* [25], which reported that the low-angle XRD pattern of bentonite typically exhibits a characteristic peak within the 2θ range of 6° to 7°. Upon pillaring, the d001 reflection peak shifted to a lower 2θ angle compared to the original bentonite. This shift indicates an increase in the interlayer spacing of the aluminosilicate layers, attributed to the intercalation of polyhydroxy cations into the bentonite interlayers.

The shift in the d001 reflection peak of Ni/PILC catalysts with Ni loadings of 5 and 10 shows changes in the 2θ angles to 5.67° and 5.74°, respectively, corresponding to basal spacings of 15.55 Å and 15.37 Å. These results are consistent with the findings of Aid *et al.* [26], who reported the d001 reflection peak of Ni/PILC catalysts at a 2θ angle of 5.5°. Similarly, the Al-Ni/PILC catalyst exhibited a d001 reflection peak at 2θ = 5.80°, corresponding to a basal spacing of 15.23 Å. In contrast, the Al/PILC catalyst did not show a detectable d001 reflection peak within the 2θ range of 5°–10°. This suggests that the peak may occur at a lower angle (2θ < 5°), indicating a significantly larger interlayer spacing. However, due to the limitations of the XRD instrument used, which has a minimum detection limit of 2θ = 5°, the peak could not be observed in the present analysis. This interpretation is supported by Nauva *et al.* [27], which reported the d001 reflection peak for Al/PILC at 2θ = 4.63°, corresponding to a basal spacing of 19.06 Å [27].

The success of the pillaring process in bentonite is indicated by an increase in interlayer spacing, demonstrating that the pillaring agents Al and Ni metals were successfully intercalated into the bentonite interlayers. The Al-Ni/PILC catalyst exhibits a smaller interlayer spacing compared to the Al/PILC catalyst. According to Gil *et al.* [28], this is attributed to diffusion resistance caused by one of the pillaring metals. Aluminium, which is present in the highest concentration among the intercalated species. Additional factors include differences in the molecular sizes of the metal species absorbed into the bentonite pores, which vary in dimension. Smaller molecules can more effectively occupy the available space within the support structure, potentially resulting in higher XRD peak intensities. Conversely, larger molecules may fill the pores less efficiently. Consequently, the interlayer spacing of the Al-Ni/PILC catalyst is nearly comparable to that of the Ni/PILC catalyst.

The wide-angle XRD analysis in Figure 3 shows that the diffraction pattern of bentonite

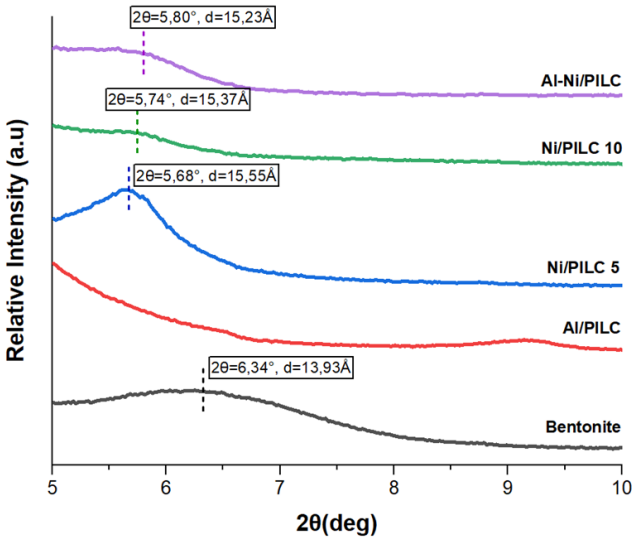

Figure 2. XRD patterns of catalysts at low angles.

exhibits prominent peaks at 2θ = 6.34°, 2θ = 20.08°, 2θ = 26.75°, and 2θ = 61.59°. These are characteristic peaks of montmorillonite, indicating that the primary component of the bentonite sample is montmorillonite, as referenced by Ref Code: 96-900-0278, which corresponds to an anorthic crystal system. This observation is supported by Dewi *et al.* [29], who reported characteristic montmorillonite peaks at 2θ = 19.58°, 20.64°, and 26.33°. Similarly, Rinaldi *et al.* [30] reported montmorillonite peaks at 2θ = 19.70°, 26.61°, 35.31°, 54.45°, and 61.69°. The modification of bentonite through the pillaring process does not significantly alter the overall montmorillonite structure. This is evidenced by the consistent presence of montmorillonite peaks in the diffractograms of all pillared samples, as shown in Figure 3.

The diffraction pattern of the Al/PILC sample reveals characteristic peaks of Al_2O_3 at 2θ = 9.454°, 18.502°, and 20.940°, based on Ref Codes 96-900-9247 and 96-900-0278, indicating that Al_2O_3 possesses an anorthic crystal system. The presence of pillared Al_2O_3 is suggested to be located within the interlayer regions of bentonite, resulting in high-intensity alumina peaks and the appearance of new detectable reflections, as shown in Figure 3. A study by Ramadhaniati *et al.* [31] on aluminum-pillared clay catalysts reported XRD peaks at 2θ = 19.83°, 20.85°, 26.64°, 35.15°, 37.40°, and 61.90°. Aluminum contains H^+ cations, which can enhance the acidity of montmorillonite and act as proton donors, contributing to the cleavage of –OH bonds in ethanol [32].

The diffraction patterns of Ni/PILC samples with molar ratios of 5 and 10 exhibit similar spectral profiles, although differences in peak intensities are observed, as shown in Figure 3.

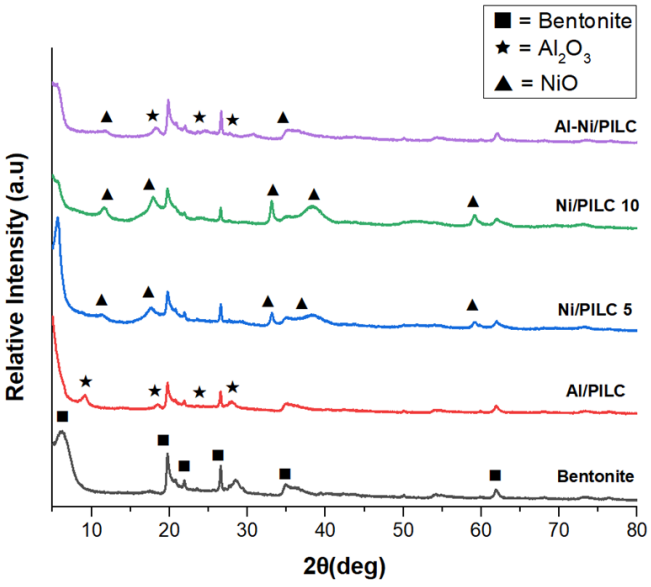

Figure 3. XRD patterns of catalysts at high angles.

The Ni/PILC sample with a ratio of 5 displays characteristic NiO peaks at 2θ = 11.439°, 33.128°, 38.592°, and 59.179°, based on Ref Codes 96-901-2318 and 96-901-1315, corresponding to a hexagonal crystal system. Similarly, the Ni/PILC sample with a ratio of 10 shows characteristic NiO peaks at 2θ = 11.433°, 33.128°, 38.592°, and 59.179°, based on Ref Codes 96-901-1315 and 96-901-2317, also corresponding to a hexagonal crystal system. These results demonstrate that an increase in the molar ratio of nickel as a pillar correlates directly with an increase in the intensity of the NiO peaks in both spectra. According to JCPDS card No. 87-0712, NiO diffraction peaks were detected in Ni/bentonite at 2θ = 37.2°, 43.3°, 62.8°, 75.4°, and 79.3° [33].

A study conducted by Lahoues-Chakour *et al.* [34] confirmed the presence of NiO supported on PILC. This was evidenced by diffraction peaks at 2θ angles of 38.50° and 37.42°, corresponding to data from ICDD#48-1548. These findings indicate the presence of oxidized NiO species. Furthermore, the results demonstrate that the active NiO sites exhibit significant exchangeability within the bentonite structure. This is further supported by the emergence of new, high-intensity peaks formed during the pillaring process [35].

The diffraction pattern of the Al-Ni/PILC sample exhibits peaks at 2θ = 5.803°, 11.439°, 18.298°, 19.747°, 26.553°, 34.588°, and 61.909°. Characteristic peaks corresponding to Al_2O_3 are observed at 2θ = 18.298° and 20.607°, based on Ref. Code 96-101-1082, which corresponds to a monoclinic crystal system. Additionally, characteristic NiO peaks appear at 2θ = 11.439° and 34.588°, referring to Ref. Code 96-901-2318, associated with a hexagonal crystal system. Overall, the XRD analysis indicates that the emergence of new peaks, shifts in peak positions, and changes in peak intensities confirm that the intercalated aluminum and nickel oxide species have been well dispersed between the bentonite layers without altering the bentonite structure [25].

3.2. XRF Analysis

The XRF analysis results presented in Table 1 indicate that bentonite is primarily composed of two main components: SiO_2 and Al_2O_3. These metal oxides dominate the bentonite composition, with percentages significantly higher than those of other metal oxides such as MgO, Fe_2O_3, Na_2O, and NiO. The contents of SiO_2 and Al_2O_3 in bentonite before pillaring were 62.57% and 23.02%, respectively. Structural modification of bentonite with aluminum and nickel oxides resulted in increased concentrations of Al_2O_3 and NiO in the Al/PILC, Ni/PILC (ratios 5 and 10), and Al-Ni/PILC catalysts.

The Ni/PILC catalysts with molar ratios of 5 and 10 also show an increase in NiO content, whereas the original bentonite not contained NiO. After pillaring, the NiO content increased to 37.53% for the Ni/PILC-5 catalyst and 53.77% for the Ni/PILC-10 catalyst. A higher mmol metal-to-gram bentonite ratio leads to greater incorporation and a more uniform distribution of pillared metals within the bentonite interlayer spaces. The combination of the two metal oxides, Al and Ni intercalated in the Al-Ni/PILC catalyst shows Al_2O_3 and NiO contents of 35.3% and 2%, respectively. In comparison, the Ni/PILC catalysts with ratios of 5 and 10 exhibit higher NiO contents of 37.53% and 53.77%, respectively. The significantly lower NiO content in the Al-Ni/PILC catalyst is attributed to diffusion limitations caused by the predominance of Al molecules intercalated as the primary metal source, resulting in a notable alteration in the distribution of metal oxides, and also reinforces the XRD analysis results, which show the characteristic peak of aluminum [25].

3.3. Surface Area Analysis

Figure 4 shows that bentonite exhibits a Type IV isotherm, supported by the data in Table 2, which indicates a pore size of approximately 12.25 nm classifying it as mesoporous. The hysteresis loop of bentonite tends to form an H3-type loop.

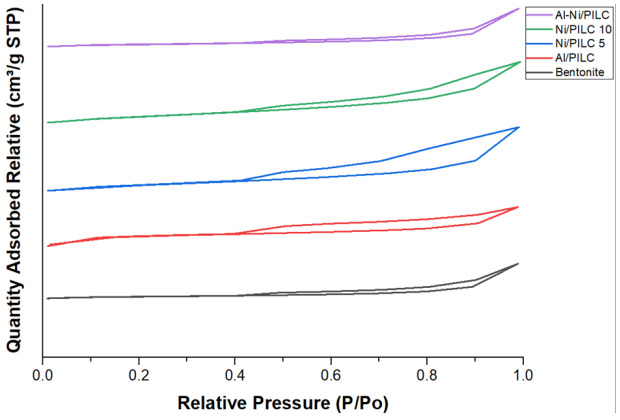

Figure 4. Nitrogen adsorption-desorption isotherms of raw and pillared bentonite.

Similarly, the Al/PILC, Ni/PILC (ratios 5 and 10), and Al-Ni/PILC catalysts also display Type IV isotherms, indicating mesoporosity with pore size ranges between 3.32 and 12.83 nm. The hysteresis loops of the Ni/PILC (ratio 10) and Al-Ni/PILC catalysts are comparable to that of bentonite and are categorized as H3-type. According to Thommes *et al.* [36], this type of hysteresis is commonly observed in materials with slit-shaped pores or aggregates of plate-like particles. H3-type hysteresis is frequently found in layered materials, such as certain types of clay, including bentonite. In contrast, the Al/PILC and Ni/PILC (ratio 5) catalysts tend to exhibit H2-type hysteresis, which indicates a narrow pore body distribution with a broader neck size distribution.

The SAA characterization results are presented in Table 2. The Table 2 presents the changes in specific surface area and pore volume of bentonite before and after the pillaring process. The unpillared bentonite exhibited a specific surface area of 26.47 m^2/g and a pore volume of 0.08 cm^3/g. After pillaring, both surface area and pore volume increased for all catalysts: 187.83 m^2/g and 0.15 cm^3/g for Al/PILC, 68.94 m^2/g and 0.15 cm^3/g for Ni/PILC with a metal ratio of 5, 77.74 m^2/g and 0.14 cm^3/g for Ni/PILC with a metal ratio of 10. The increase in surface area and total pore volume after pillaring is attributed to the opening of the natural bentonite pores, resulting from the dissolution of impurities that previously blocked the pore openings. These pores were subsequently occupied by the pillar metal species [37].

The Al-Ni/PILC catalyst exhibited a lower surface area compared to Al/PILC, likely due to

Table 2. N_2 gas adsorption results by BET method.

Samples	Surface area (m^2/g)	Pore volume (cm^3/g)	Pore diameter (nm)
Bentonite	26.47	0.08	12.25
Al/PILC	187.83	0.15	3.32
Ni/PILC rasio 5	68.94	0.15	8.88
Ni/PILC rasio 10	77.74	0.14	7.92
Al-Ni/PILC	27.80	0.09	12.83

Table 1. Chemical composition of various catalyst and the support.

Samples	Elements (wt.%)					
	SiO_2	Al_2O_3	NiO	MgO	Fe_2O_3	Na_2O
Bentonite	62.57	23.02	-	3.63	5	2.11
Al/PILC	58.48	30.79	-	3.39	4.75	0.63
Ni/PILC ratio 5	39.95	14.73	37.53	1.88	2.99	-
Ni/PILC ratio 10	29.55	10.69	53.77	1.22	2.17	-
Al-Ni/PILC	52.7	35.3	2	3	4.1	0.80

uneven distribution and agglomeration of Al and Ni metals, particularly at pore mouths or channels, which blocked the pores [29]. Despite this, the surface area of Al-Ni/PILC remained higher than that of bentonite, indicating that the incorporation of Al and Ni metals within the bentonite interlayers still enhances surface area. Among the four catalysts tested, Al/PILC showed the highest surface area of 187.83 m²/g, consistent with low-angle XRD results indicating the largest interlayer spacing.

The observed increase in surface area of the catalysts indicates that Al^{3+} and Ni^{2+} cations are stably incorporated within the bentonite interlayers. The addition of transition metals such as Al and Ni enhances the catalyst surface area because, during the pillaring process, these metals are likely dispersed between the bentonite layers, leading to increased surface area, pore size, and pore volume. A high catalyst surface area provides an increased contact area and more active metal sites for interaction between ethanol and the catalyst [38]. Ethanol molecules freely diffuse before adsorbing onto the catalyst surface, where they become activated and react with the active sites of Al and Ni metals, resulting in the formation of gasoline.

3.4. FTIR Analysis

Figure 5 presents the FTIR absorption spectra of bentonite before and after pillaring with Al and Ni metals. The analysis reveals characteristic vibrational bands corresponding to various functional groups at specific wavenumbers. The FTIR spectrum analysis presented in Figure 5 reveals five characteristic absorption peaks of bentonite at wavenumbers 522.5 cm^{-1}, 619 cm^{-1}, 1011.1 cm^{-1}, 1634.2 cm^{-1}, and 3627.6 cm^{-1}. The peak at 3627.6 cm^{-1} corresponds to –OH stretching vibrations. According to Khairina *et al.* [39], this peak is attributed to the –OH stretching vibration of silanol groups situated between the tetrahedral and octahedral sheets. The absorption peak at 1634.2 cm^{-1} is assigned to the bending vibration of O–H from water molecules adsorbed within the bentonite interlayers [40]. The peak at 1011.1 cm^{-1} is indicative of Si–O–Si stretching vibrations, which Siregar and Irma [41] reported to typically occur near 1041 cm^{-1}. Additionally, the absorption at 919.6 cm^{-1} corresponds to the bending vibration of Al–Al–OH groups bonded to Al^{3+} ions. Finiels *et al.* [35] noted that the band near 918 cm^{-1} is characteristic of hydroxyl bending vibrations in the Al–Al–OH structure.

An absorption peak observed at 796.6 cm^{-1} corresponds to the bending vibration of the Si–O bond. This finding is consistent with previous studies reporting Si–O bending vibrations near 795 cm^{-1}, attributed to quartz and silica, the primary components of natural bentonite [42]. The peak at 619 cm^{-1} indicates the bending vibration of Mg–OH, in agreement with Wang *et al.* [43], who reported Mg–OH bending vibrations

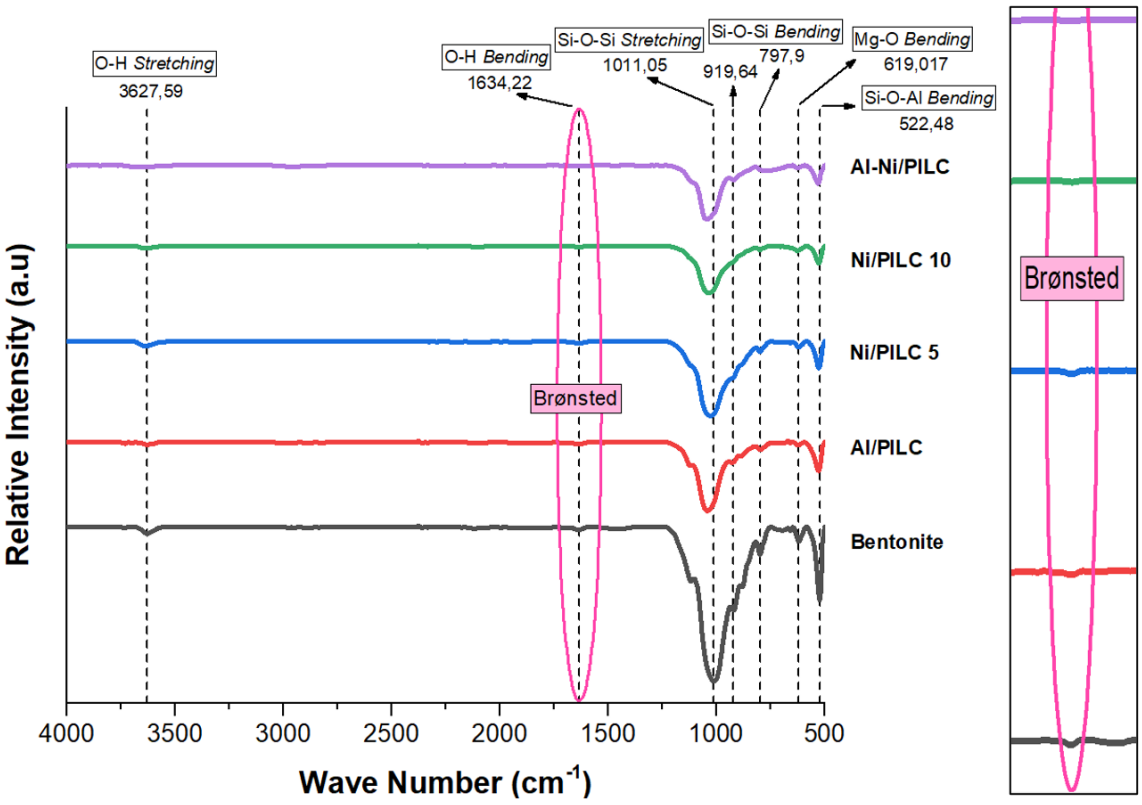

Figure 5. FTIR spectra of catalysts and enlargement of the image section.

around 623 cm^{-1}. The absorption at 522.5 cm^{-1} corresponds to the bending vibration of the Si–O–Al bond, as noted by Ruslan *et al*. [44], who identified this band near 524.54 cm^{-1}. Figure 5 presents changes in the intensity of characteristic bentonite absorption peaks following pillaring of the Al/PILC, Ni/PILC (ratios 5 and 10), and Al-Ni/PILC catalysts.

Prior studies conducted by Widjaya *et al*. [25] explained that the intensity changes observed near 1634 cm^{-1} result from the calcination process at 400 °C, during which the amount of adsorbed or coordinated water decreases due to dehydration and dehydroxylation. The reduced intensity at 1011.05 cm^{-1}, 919.64 cm^{-1}, 797.9 cm^{-1}, and 522.5 cm^{-1} corresponding to Si–O–Si and Si–O–Al groups is attributed to cation exchange between bentonite and the introduced metal oxides. FTIR analysis is also valuable for identifying the types of acidity present in catalysts. Typically, catalysts exhibit two types of acid sites, i.e. Brønsted and Lewis acid sites. The Brønsted acidity is observed at wavenumbers between 1515 and 1640 cm^{-1}, whereas the Lewis acidity appears between 1435 and 1470 cm^{-1}. Brønsted acid sites originate from silanol groups within the bentonite structure, which act as proton (H^+) donors. In contrast, Lewis acid sites are associated with metal oxide pillars that act as electron pair acceptors. The conversion of ethanol to gasoline proceeds efficiently when the catalyst exhibits Brønsted acidity, functioning as a proton donor. FTIR absorption peaks for bentonite, Al/PILC, Ni/PILC (ratios 5 and 10), and Al-Ni/PILC, confirm the presence of Brønsted acid sites. Rinaldi and Dwiatmoko [3] reported that the ethanol to gasoline conversion reaction is enhanced by catalysts with a high density of proton donors or strong Brønsted acidity.

The FTIR analysis supports and complements the XRD results, confirming the structural and compositional changes that occurred after the pillaring process. The XRD patterns previously indicated an increase in interlayer spacing and the appearance of characteristic peaks associated with Al and Ni species, signifying the successful incorporation of metal oxides into the bentonite framework. Correspondingly, the FTIR spectra showed decreased intensity of Si–O–Si and Si–O–Al vibration bands, reflecting structural modification of the tetrahedral–octahedral layers due to cation exchange and pillar formation. Furthermore, the emergence and shift of absorption bands related to metal–oxygen (Al–O and Ni–O) vibrations corroborate the presence of aluminum and nickel pillars observed in the XRD patterns. These findings collectively verify that the pillaring process not only alters the crystalline structure, as evidenced by XRD, but also modifies the chemical bonding environment, as revealed by FTIR, leading to enhanced surface acidity beneficial for catalytic performance.

Table 3. Acidity of various catalysts and their supports.

Samples	Acidity (mmol/g)
Bentonite	2.29
Al/PILC	2.34
Ni/PILC 5	2.12
Ni/PILC 10	2.26
Al-Ni/PILC	2.33

3.5. TPD-NH_3 Analysis

The acidity site absorption peaks observed for bentonite, Al/PILC, Ni/PILC with ratios of 5 and 10, as well as Al-Ni/PILC, as shown in Figure 6, exhibit two distinct peaks corresponding to the acid strength of the catalysts. According to Binitha and Sugunan [45], catalyst acidity can be classified into three categories based on desorption temperature: weak acid sites (100–200 °C), medium acid sites (200–400 °C), and strong acid sites (400–600 °C). The TPD-NH_3 analysis curves for bentonite, Al-Ni/PILC with ratios of 5 and 10, and Al-Ni/PILC display prominent peaks at higher temperatures, indicating a predominance of strong acid sites. Total acidity analysis using TPD employs NH_3 gas as a basic adsorbate, which interacts with the acid sites of the catalyst to form NH_4^+ species. The amount of NH_3 adsorbed reflects the total acidity of the catalyst.

The total acidity values for the catalysts are summarized in Table 3. Table 3 shows TPD-NH_3 analysis results for the Al/PILC and Al-Ni/PILC catalysts, with values of 2.34 mmol/g and 2.33 mmol/g, respectively. Although the increase in total acidity appears relatively small (approximately 2%), the reproducibility of the TPD-NH_3 measurements and the consistent trend observed across repeated analyses indicate that the change is significant. This slight increase in total acidity is consistent with the introduction of Al and Ni oxide pillars, which contribute to the formation of additional Lewis and Brønsted acid sites, as supported by the FTIR and XRD analyses. Previous studies have also reported relatively small yet meaningful increases in acidity following the pillaring process with metal oxides, indicating structural stabilization and improved accessibility of acid sites rather than a drastic increase in their quantity. Therefore, the observed change, although numerically minor, reflects a real modification of the catalyst's surface properties that positively influences its catalytic performance. In contrast, the Ni/PILC catalysts with ratios of 5 and 10 exhibit a decrease in total acidity compared to Al/PILC. This difference can be attributed to the electronic configuration of the pillaring metal. Nickel has

only one vacant orbital, whereas aluminum possesses two vacant orbitals, making it more capable of accepting electron pairs. According to Fatimah *et al.* [46], catalysts incorporating pillaring metals with a greater number of vacant d-orbitals tend to exhibit higher acidity. Differences in total acidity are also influenced by ion or cation exchange within the interlayer space of bentonite, which is affected by the oxidation state and charge of the pillaring metal. A stronger positive character of the metal cation enhances the acid strength generated.

PILC catalysts containing mixed metal oxide pillars of Al and Ni exhibit higher acidity than those with single metal oxide pillars. The combination of two different metal oxides can produce a synergistic effect due to interactions between the two oxide pillars. These interactions can result in the formation of a greater number of stronger acid sites, thereby enhancing the overall acidity. The increase in total acidity of the catalyst correlates positively with enhanced selectivity. A greater amount of NH_3 adsorbed by the catalyst corresponds to stronger acidity and higher catalytic activity. These findings highlight the critical role of acidity in determining the catalytic performance of the material [47]. Catalysts exhibiting higher total acidity, as indicated by greater NH_3 desorption, demonstrate improved catalytic performance and product selectivity in the GC-FID analysis. This relationship suggests that stronger and more abundant acid sites

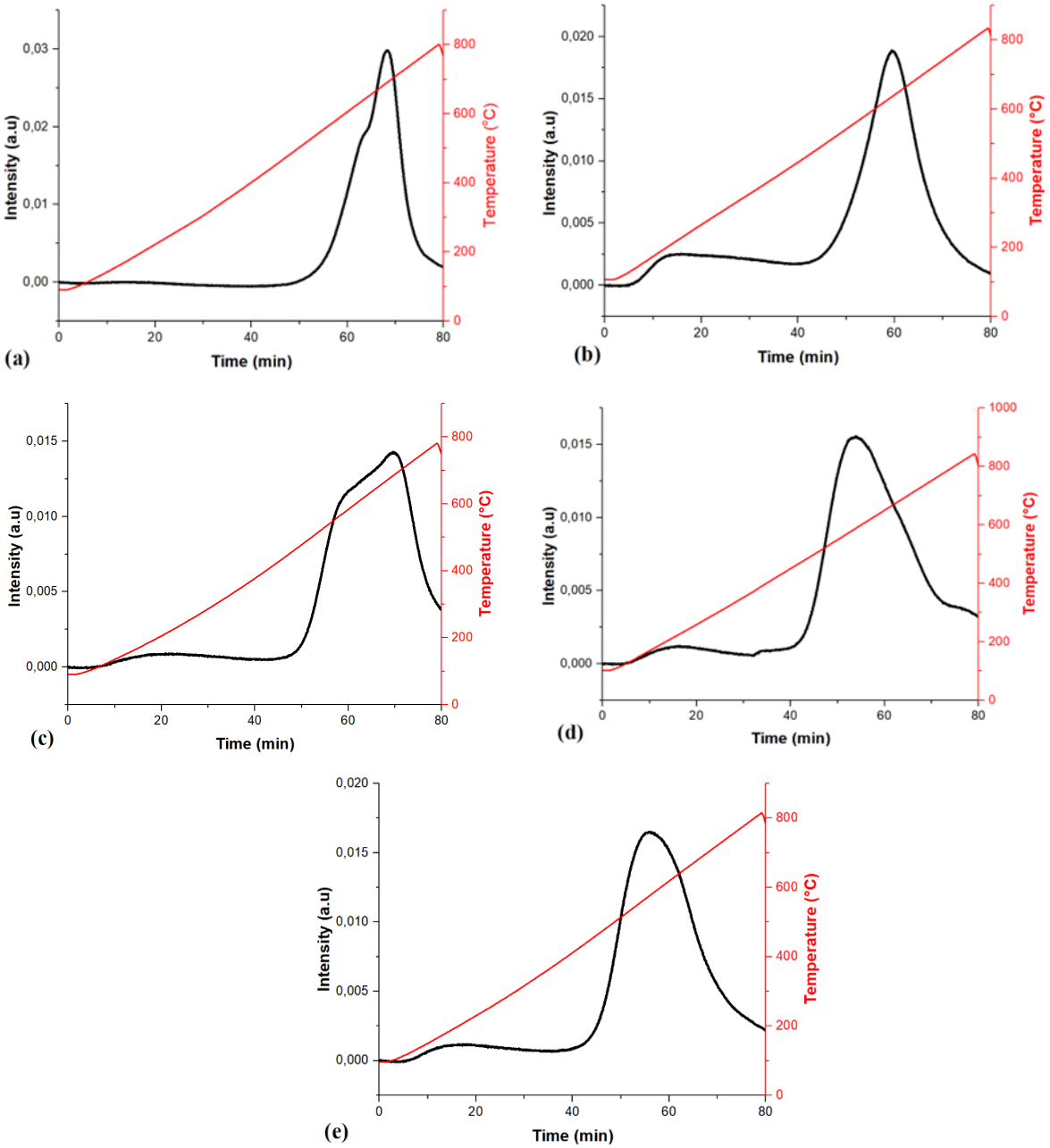

Figure 6. Total acidity profile of the catalyst based on NH_3-TPD: (a) Bentonite, (b) Al/PILC, (c) Ni/PILC with ratio of 5, (d) Ni/PILC with ratio of 10, (e) Al-Ni/PILC.

facilitate the conversion of ethanol to hydrocarbons, resulting in higher yield and selectivity toward gasoline-range products. Thus, the TPD-NH_3 and GC-FID analyses collectively confirm that the catalytic activity is strongly governed by the surface acidity characteristics of the catalyst.

The shift of acid sites toward lower strength after the pillaring process is consistent with the partial modification of the bentonite framework, where the introduction of metal oxide pillars alters the distribution of surface acidity. Although a decrease in acid strength is observed, this transformation may enhance the accessibility and dispersion of active sites, facilitating better interaction between the reactant molecules and the catalyst surface. Moreover, moderate acid sites are often favorable for ethanol conversion reactions, as excessively strong acid sites can promote unwanted side reactions such as coke formation. Therefore, the observed redistribution of acid sites reflects a balance between strength and accessibility, which can contribute positively to catalytic stability and selectivity.

3.6. TGA Analysis

Table 4 presents the analysis of catalyst mass reduction over the three stages of the reaction. The relative mass loss of bentonite, Al/PILC, Ni/PILC (with ratios of 5 and 10), and Al-Ni/PILC as the temperature increases up to 1000 °C, with corresponding values of 4.88%, 12.62%, 4.02%, 6.99%, and 10.76%, respectively. The first stage corresponds to the physical release of water molecules (dehydration) from the surface of the catalyst structure. Bentonite shows a mass loss of 2.05% within the temperature range of 50–95 °C. In the second stage, bentonite exhibits a mass loss of 2.62% within the temperature range of 95–701 °C, while the Al/PILC, Ni/PILC (ratios of 5 and 10), and Al-Ni/PILC catalysts show mass losses ranging from 2.54% to 7.20% between 92–701 °C. These temperature ranges correspond to dehydroxylation and structural transformation of salt species in the cationic oligomers within the bentonite interlayers [47].

The third stage is associated with chemical decomposition. Bentonite undergoes a mass loss of 0.21% between 701–1000 °C, while the Al/PILC, Ni/PILC (ratios of 5 and 10), and Al-Ni/PILC catalysts exhibit mass losses ranging from 0.65% to 6.38% in the range of 441–815 °C. At this stage, the samples demonstrate inert behavior, with only minor mass reduction observed. According to Fayisa *et al*. [48], maximum dehydroxylation of the pillared metal species within the bentonite interlayers occurs between 500–680 °C, leading to degradation of the alumina–silica framework in the bentonite. The Al-Ni/PILC catalyst demonstrates greater thermal stability compared to single-metal catalysts, attributed to the synergistic interaction between aluminum and nickel, which enhances overall structural integrity. The modification of bentonite by incorporating both Al and Ni improves the physical robustness of the bentonite framework, thereby enhancing the thermal stability of the catalyst material [49].

3.7. GC-FID Analysis

Based on Figure 7, ethanol was successfully converted into gasoline-range compounds, as evidenced by the increased conversion percentage compared to the initial bentonite. At a temperature of 150 °C, the highest conversion was achieved using the Al/PILC catalyst, with a conversion rate of 71.65%. According to BET analysis, the Al/PILC catalyst possesses a larger specific surface area and pore volume than the Ni/PILC catalysts with ratios of 5 and 10, as well as the Al-Ni/PILC catalyst. (Ramadhaniati et al., 2023) [31] reported that a higher specific surface area and pore volume facilitate greater ethanol diffusion and interaction within the bentonite structure. FTIR analysis of the Al/PILC catalyst confirmed the presence of Brønsted acid sites. A high level of acidity is essential for the effective conversion of ethanol to gasoline. Brønsted acid sites act as the primary active sites in the ethanol-to-gasoline conversion process.

The successful conversion of ethanol to gasoline-range compounds was also observed at a

Table 4. Results of thermogravimetric analysis.

Samples	Stage 1		Stage 2		Stage 3	
	Temperature (°C)	Mass Reduction (%)	Temperature (°C)	Mass Reduction (%)	Temperature (°C)	Mass Reduction (%)
Bentonite	50-95	2.05	95-701	2.62	701-1000	0.21
Al/PILC	41-100	3.21	100-665	7.20	665-1000	2.21
Ni/PILC 5	59-89	0.83	89-690	2.54	690-1000	0.65
Ni/PILC 10	45-70	0.59	70-570	3.51	570-1000	2.89
Al-Ni/PILC	58-92	0.53	92-441	3.85	441-1000	6.38

temperature of 250 °C. As shown in Figure 7, the highest conversion at this temperature was achieved using the Al-Ni/PILC catalyst, with a conversion rate of 70.96%. This increase in conversion can be attributed to the influence of temperature on catalytic activity. Acidity analysis using NH_3-TPD revealed that the Al-Ni/PILC catalyst possessed a relatively high level of acidity, attributed to the synergistic effect of Al and Ni as active metal components. FTIR analysis further confirmed the presence of Brønsted acid sites, which play a critical role as active sites in the ethanol-to-gasoline conversion reaction [47].

The Al/PILC catalyst showed a decrease in conversion efficiency at 250 °C. According to Widjaya *et al.* [50], this may be due to the effect of high temperatures, which can lead to the formation of residues that block the active sites of the catalyst, thereby diminishing its catalytic activity. The decrease in ethanol-to-gasoline conversion observed for the Al/PILC catalyst with increasing temperature (150–250 °C) can be attributed to structural and surface transformations that occur in the absence of metallic promoters. At elevated temperatures, partial dehydroxylation of alumina pillars likely reduces both the number and strength of Brønsted acid sites, which are crucial for ethanol dehydration and subsequent hydrocarbon formation. In addition, the absence of metal species such as Ni limits hydrogen transfer reactions, thereby promoting the accumulation of oxygenated intermediates and carbonaceous residues that progressively block the active sites. These combined effects lead to a noticeable decline in catalytic efficiency for Al/PILC at higher temperatures, contrasting with the enhanced activity observed for metal-modified catalysts. This finding underscores the essential role of metal incorporation in preserving active site accessibility and thermal stability, as elaborated in the catalytic performance discussion. The selectivity analysis of the compounds produced from the ethanol-to-gasoline conversion, as determined by GC-FID, is presented in Tables 5 and 6.

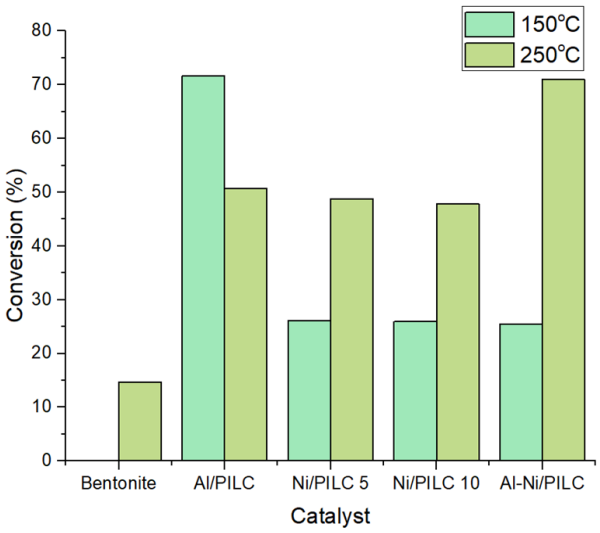

Figure 7. Catalytic reaction test results.

The analysis presented in Tables 5 and 6 demonstrates that the ethanol-to-gasoline conversion process produced hydrocarbon compounds in the C_6–C_{12} range, consisting primarily of paraffinic and aromatic species. These compounds represent the main constituents of commercial gasoline, as previously verified. As shown in Table 5, the Al/PILC catalyst exhibited the highest gasoline selectivity at a reaction temperature of 150 °C, achieving 59.25%, with the highest product selectivity observed for *n*-heptane (C_7H_{16}) at 59.06%. In Table 6, the Al-Ni/PILC

Table 5. Selectivity analysis of ethanol conversion products to gasoline using GC-FID at 150 °C.

Catalyst	Selectivity (%)				
	Bentonite	Al/PILC	Ni/PILC 5	Ni/PILC 10	Al-Ni/PILC
n-Heptane (C_7H_{16})	0.87	59.07	0.01	0.26	0.01
Cyclohexane (C_6H_{12})	0.01	0.13	20.20	21.01	18.62
Toluene (C_7H_8)	0.01	0.05	0.04	0.14	0.01
Selectivity of Gasoline	0.89	59.25	20.25	21.41	18.64

Table 6. Selectivity analysis of ethanol conversion products to gasoline using GC-FID at 250 °C.

Catalyst	Selectivity (%)				
	Bentonite	Al/PILC	Ni/PILC 5	Ni/PILC 10	Al-Ni/PILC
n-Heptane (C_7H_{16})	4.30	4.27	9.54	10.68	23.48
Cyclohexane (C_6H_{12})	0.03	0.03	0.14	0.45	0
Toluene (C_7H_8)	0	0.36	0.31	0.24	0.15
n-Dodecane ($C_{12}H_{26}$)	1.03	0.03	0.13	0.38	0
Selectivity of Gasoline	5.36	4.69	10.12	11.75	23.63

catalyst showed the highest gasoline selectivity at a reaction temperature of 250 °C, reaching 23.63%, with *n*-heptane (C_7H_{16}) again being the most selectively produced compound at 23.48%. The reaction results indicate that using aluminum and nickel is more advantageous than using tin and chromium, as the selectivity achieved with aluminum and nickel reaches up to 59%, whereas with tin and chromium in the previous studies, it is only 22%.

The selectivity toward gasoline-range hydrocarbons was calculated on a carbon-mole basis, defined as the ratio between the moles of carbon in the gasoline fraction (C_5–C_{12} hydrocarbons) and the total moles of carbon in all detected products in the liquid phase. Gasoline selectivity was determined from the hydrocarbon distribution obtained by GC–FID analysis. In addition to gasoline-range compounds, minor fractions of light olefins (C_2–C_4) may also be present. However, gas-phase samples were not collected during the catalytic tests, and thus the gaseous products were vented. A portion of the remaining products consisted of unconverted ethanol. The formation of gaseous products such as ethylene and light olefins indicates that secondary reactions, including cracking and dehydration, also occur during ethanol conversion, consistent with previously reported mechanisms.

A high acidity level in the catalyst is essential for the ethanol-to-gasoline conversion process. The presence of H^+ ions, serving as the acid sites, plays a critical role in cleaving C–O bonds during the dehydration step and facilitating the formation of hydrocarbon chains through oligomerization, ultimately producing gasoline-range compounds with extended hydrocarbon chains [51]. The mechanism of ethanol conversion to gasoline involves three main stages. The first stage is the dehydration of ethanol to produce ethylene, the simplest olefin. The second stage involves oligomerization, where ethylene molecules combine to form olefins with longer hydrocarbon chains. In the final stage, hydrogenation converts these olefins into paraffinic compounds, while dehydrocyclization leads to the formation of aromatic compounds, with hydrocarbon chain lengths ranging from C_5 to C_{12}.

Based on the comprehensive GC-FID analysis, it can be concluded that reaction temperature significantly influences the ethanol-to-gasoline conversion process. The Al/PILC catalyst was identified as the most effective catalyst for ethanol conversion at 150 °C, characterized by high total acidity and the presence of Brønsted acid sites. Upon increasing the temperature to 250 °C, the bimetallic Al-Ni/PILC catalyst demonstrated synergistic effects that enhanced the performance of the active metals and suppressed undesired side reactions, thereby achieving optimal catalytic activity and selectivity at elevated temperatures.

4. Conclusions

The characterization results confirmed that the pillaring of bentonite with aluminum (Al), nickel (Ni), and a combination of Al–Ni metals in the Al/PILC, Ni/PILC (Ni ratios of 5 and 10), and Al–Ni/PILC catalysts successfully enhanced the physicochemical properties of the materials. The interlayer spacing increased to 15.55, 15.37, and 15.23 Å, respectively, indicating the successful intercalation of metal oxide pillars into the bentonite layers. The specific surface areas were 187.83, 68.94, 77.74, and 27.80 $m^2.g^{-1}$, while the corresponding pore volumes were 3.32, 8.88, 7.92, and 12.83 $cm^3.g^{-1}$. The total acidity values were measured at 2.34 $mmol.g^{-1}$ for Al/PILC and 2.33 $mmol.g^{-1}$ for Al–Ni/PILC, confirming the enhancement of acid sites due to metal incorporation.nReaction temperature was found to significantly affect both catalytic activity and selectivity in the ethanol-to-gasoline (ETG) conversion process. At 150 °C, the Al/PILC catalyst exhibited the most favorable performance, achieving an ethanol conversion of 71.65% and a gasoline-range hydrocarbon selectivity of 59.25%. In contrast, at an elevated temperature of 250 °C, the Al–Ni/PILC catalyst demonstrated improved overall activity, yielding a conversion of 70.96% with a selectivity of 23.63%. These findings suggest that the introduction of nickel in conjunction with aluminum enhances the catalyst's thermal stability and modifies its acid characteristics, thereby influencing product distribution at higher reaction temperatures. Overall, the results indicate that aluminum contributes predominantly to the development of strong acid sites essential for hydrocarbon chain growth at moderate temperatures, while nickel enhances thermal stability and hydrogen transfer reactions under harsher conditions. The combined Al–Ni pillaring strategy thus provides a promising approach for tuning acidity and redox functionality in bentonite-based catalysts for ethanol-to-gasoline conversion.

Acknowledgment

The authors would like to acknowledge financial support from the BRIN through Scheme of Riset & Inovasi untuk Indonesia Maju (RIIM), contract number B-6952/III.10/KS.00.00/6/2022 and the funding scheme of the nanotechnology and materials research organization (RP-ORNM

BRIN). The Indonesian Endowment Fund for Education (LPDP) also partly funded this study.

CRedit Author Statement

Author Contributions: RRW: Conceptualization, Methodology, Investigation, Resources, Data Curation, Writing, Review and Editing, Supervision, Project Administration, Resources; YDIS: Methodology, Investigation, Writing, Review and Editing; SHN: Data Curation, Writing Draft Preparation; NR: Validation, Resources; SPS: Review and Editing; JP: Validation, Resources; AAD: Validation, Resources. All authors have read and agreed to the published version of the manuscript.

References

[1] Robinson, P.R. Petrochemicals. In *Petroleum Science and Technology: Downstream*; Springer, 2024; pp. 243–291. https://link.springer.com/book/10.1007/978-3-031-46645-8.

[2] International Energy Agency. (2023). *World Energy Outlook 2023*. Paris: IEA. https://www.iea.org/reports/world-energy-outlook-2023

[3] Rinaldi, N., Dwiatmoko, A.A. (2011). Studi Awal Pada Preparasi Katalis Berbasis Lempung Berpilar Untuk Reaksi Etanol Menjadi Gasoline (Etg). *Jurnal Kimia Terapan Indonesia*, 13(2), URL: http://inajac.lipi.go.id/index.php/InaJAC/article/view/155/164

[4] Li, X., Zhang, C., Zhang, X., Wang, S., Meng, Q., Wu, S., Yang, H., Xia, Y., Chen, R. (2016). An acetyl-L-carnitine switch on mitochondrial dysfunction and rescue in the metabolomics study on aluminum oxide nanoparticles. *Particle and Fibre Toxicology*, 13(1), 4. DOI: 10.1186/s12989-016-0115-y.

[5] Shi, D., Wojcieszak, R., Paul, S., Marceau, E. (2019). Ni promotion by Fe: What benefits for catalytic hydrogenation? *Catalysts,* 9(5), 451. DOI: 10.3390/catal9050451

[6] Aboul-Gheit, A.K., Gad, F.K., Abdel-Aleem, G.M., El-Desouki, D.S., Hmaid, S.M.A., Ghoniem, S.A., Ibrahim, A.H. (2014). Pt, Re and Pt-Re incorporation in sulfated zirconia as catalyst for pentane isomeration. *Egypt. J. Pet.* 23, 303–314. DOI: 10.1016/j.ejpe.2014.08.006.

[7] Demirci, Ü.B., Garin, F. (2002). Kinetic study of n-heptane conversion on sulfated zirconia-supported platinum catalyst: the metal-proton adduct is the active site. *J. Mol. Catal. A Chem.* 188, 233–243, DOI: 10.1016/S1381-1169(02)00337-0.

[8] Veiga, S., Bussi, J. (2016). Steam reforming of crude glycerol over nickel supported on activated carbon. *Energy Convers. Manag.* 141, 79–84. DOI: 10.1016/j.enconman.2016.04.103

[9] Shah, A.K., Malviya, N., Korde, S.R., Dalai, A.K. (2023). Design of nickel supported hierarchical ZSM-5/USY zeolite bifunctional catalysts for one-pot menthol synthesis. *Molecules,* 28(2), 743. DOI: 10.3390/molecules28020743

[10] Kadarwarti, S., Rahmawati, F., Rahyu, P.E., Wahyuni, S., Supardi, K.I. (2013). Kinetics and mechanism of Ni/zeolite-catalyzed hydrocracking of palm oil into biofuel. *Indones. J. Chem*. 13 (1), 77–85. DOI: 10.22146/ijc.21330.

[11] Suseno, A., Wijaya, K., Trisunaryanti, W., Roto. (2018). Synthesis and characterization of Ni- Cu doped zirconia-pillared bentonite. *Orient. J. Chem*. 34 (3), 1–5. DOI: 10.13005/ojc/340332.

[12] Balcı, S. (2017). Structural property improvements of bentonite with sulfuric acid activation. *Journal of the Turkish Chemical Society Section B: Chemical Engineering*, 1(1), 19–32. DOI: 10.18596/jotcsb.31081

[13] Souza, L.K.C., Santos, A.C., Batista, E.A.C., Meirelles, A.J.A. (2013). Liquid–liquid equilibrium for systems containing ethanol, water, and essential oils. *Fluid Phase Equilibria,* 337*,* 67–75. DOI: 10.1016/j.fluid.2012.09.022

[14] Du, W., Slany, M., Wang, X., Chen, G., Zhang, J. (2020). The inhibition property and mechanism of a novel low molecular weight zwitterionic copolymer for improving wellbore stability, *Polymers* 12, 708. DOI: 10.3390/polym12030708.

[15] Du, W., Wang, X., Chen, G., Zhang, J., Slany, M. (2020). Synthesis, property and mechanism analysis of a novel polyhydroxy organic amine shale hydration inhibitor. *Minerals,* 10, 128. DOI: 10.3390/min10020128.

[16] Maes N., Heylen I., Cool P., Vasant E.F. (1997). The relation between the synthesis of pillared clay and their resulting porosity. *J. Appl. Clay Sci.* 12, 43–60. DOI: 10.1016/S0169-1317(96)00036-1.

[17] Wang, Q., Shaheen, S.M., Jiang, Y., Li, R., Slany, M., Abdelrahman, H., Kwon, E., Bolan, N., Rinklebe, J., Zhang, Z. (2020). Fe/Mn- and P-modified drinking water treatment residuals reduced Cu and Pb phytoavailability and uptake in a mining soil. *J. Hazard. Mater.*, 403, 123628. DOI: 10.1016/j.jhazmat.2020.123628.

[18] Leffler, T., Brackmann, C., Berg, M., Aldén, M., Li, Z. (2017). Online Alkali Measurement during Oxy-fuel Combustion. *Energy Procedia*, 120, 365–372, DOI: 10.1016/j.egypro.2017.07.217.

[19] Rinaldi, R., Schüth, F. (2009). Design of solid catalysts for the conversion of biomass. *Energy & Environmental Science*, 2(6), 610–626. DOI: 10.1039/B902668A.

[20] Wahyuningsih, P. (2022). Bentonit Tersulfatasi sebagai Katalis dalam Produksi Biodiesel dari Minyak Jelantah. *QUIMICA: Jurnal Kimia Sains dan Terapan*, 4(1), 5–8. DOI: 10.33059/jq.v4i1.4377.

[21] Machado, N.R.C.F., Calsavara, V., Astrath, N.G.C., Matsuda, C.K., Paesano, A., Baesso, M.L. (2005). Obtaining hydrocarbons from ethanol over iron-modified ZSM-5 zeolites. *Fuel*, 84(16), 2064–2070. DOI: 10.1016/j.fuel.2005.05.001.

[22] Kloprogge, J.T., Duong, L.V., & Frost, R.L. (2005). A review of the synthesis and characterisation of pillared clays and related porous materials for cracking of vegetable oils to produce biofuels. *Environmental Geology*, 47(7), 967–981. DOI: 10.1007/s00254-005-1226-1.

[23] Suseno, A. (2019). Hydrocracking of palm oil to gasoline on bimetallic Ni-Cu/zirconia pillared bentonite. *IOP Conference Series: Materials Science and Engineering*, 509, 012005. DOI: 10.1088/1757-899X/509/1/012005.

[24] Galeano, L.-A., Vicente, M. Á., & Gil, A. (2014). Catalytic Degradation of Organic Pollutants in Aqueous Streams by Mixed Al/M-Pillared Clays (M = Fe, Cu, Mn). *Catalysis Reviews*, 56(3), 239–287. DOI: 10.1080/01614940.2014.904182.

[25] Widjaya, R.R., Saridewi, N., Putri, A.A., Rinaldi, N., & Dwiatmoko, A.A. (2021). Fe-Cr pillared clay as catalysts for the ethanol to gasoline conversion. *IOP Conference Series: Materials Science and Engineering*, 1011(1). DOI: 10.1088/1757-899X/1011/1/012008.

[26] Aid, A., Andrei, R.D., Amokrane, S., Cammarano, C., Nibou, D., & Hulea, V. (2017). Ni-exchanged cationic clays as novel heterogeneous catalysts for selective ethylene oligomerization. *Applied Clay Science*, 146, 432–438. DOI: 10.1016/j.clay.2017.06.034.

[27] Nauva, F., Santosa, S.J., Prasetya, A., & Siswoyo, E. (2015). Synthesis and characterization of Al-pillared bentonite and its application for phenol adsorption. *Indonesian Journal of Chemistry*, 15(1), 37–46. DOI: 10.22146/ijc.21210

[28] Gil, A., Korili, S.A., & Vicente, M.A. (2008). Recent advances in the control and characterization of the porous structure of pillared clay catalysts. In *Catalysis Reviews - Science and Engineering,* 50, 2, 153–221. DOI: 10.1080/01614940802019383.

[29] Dewi, D.A.D.N., Simpen, I.N., & Suarsa, I.W. (2020). Synthesis And Characterization Of Photocatalys Fe2O3 Pillared Montmorillonite Doped TiO2 And Its Application For Rhodamine B Phododegradation Using Visible Light Irradiation. *Jurnal Kimia*, 82. DOI: 10.24843/jchem.2020.v14.i01.p14.

[30] Rinaldi, N., Sari, N.L., Sumari, S., Kristiani, A., Agustian, E., Widjaya, R.R., & Dwiatmoko, A. (2024). Performance of sulfided NiMo catalyst supported on pillared bentonite Al and Ti under hydrodeoxygenation reaction of guaiacol. *International Journal of Renewable Energy Development*, 13(3), 539–548. DOI: 10.61435/ijred.2024.60060.

[31] Ramadhaniati, D., Saridewi, N., Dwiatmoko, A. A., Rinaldi, N., Ramdani, D., Putri, A.M.H., & Widjaya, R.R. (2023). Aluminium and zirconium pillared bentonite for ethanol to gasoline conversion process. *In AIP Conference Proceedings*, 2947, Vol. 2902-No.1. DOI: 10.1063/5.0173147.

[32] Widjaya, R.R., Soegijono, B., & Rinaldi, N. (2012). Characterization of Cr/Bentonite and HZSM-5 Zeolite as Catalysts for Ethanol Conversion to Biogasoline. *Makara Journal of Science*, 16(1), 65–70. DOI: 10.7454/mss.v16i1.1283.

[33] Jiang, Y., Huang, T., Dong, L., Qin, Z., & Ji, H. (2018). Ni/bentonite catalysts prepared by solution combustion method for CO2 methanation. *Chinese Journal of Chemical Engineering*, 2361–2367. DOI: 10.1016/j.cjche.2018.03.029.

[34] Lahoues-Chakour, N., Barama, S., Barama, A., Djellouli, B., Domingos, C., & Davidson, A. (2018). Catalytic behavior of nickel loaded on acid-activated and pillared clay in total gas-phase oxidation of ethanol. *Journal of Nanoparticle Research*, 20(11). DOI: 10.1007/s11051-018-4385-1.

[35] Finiels, A., Fajula, F., & Hulea, V. (2014). Nickel-based solid catalysts for ethylene oligomerization – a review. *Catal. Sci. Technol.*, 4(8), 2412–2426. DOI: 10.1039/C4CY00305E.

[36] Thommes, M., Kaneko, K., Neimark, A.V., Olivier, J.P., Rodriguez-Reinoso, F., Rouquerol, J., & Sing, K.S.W. (2015). Physisorption of gases, with special reference to the evaluation of surface area and pore size distribution (IUPAC Technical Report). *Pure and Applied Chemistry*, 87(9–10), 1051–1069. DOI: 10.1515/pac-2014-1117.

[37] Saraswati T.E., Bahrudin A., Anwar M. (2016). Effects of Heating Temperature and Binder in the Production of Char-Based Electrical Conductor. *ALCHEMY Jurnal Penelitian Kimia*, 12(2), 167-178. DOI: 10.20961/alchemy.v12i2.708.

[38] Armaroli, T., Simon, L. J., Digne, M., Montanari, T., Bevilacqua, M., Valtchev, V., Patarin, J., & Busca, G. (2006) Effects of crystal size and Si/Al ratio on the surface properties of H-ZSM-5 zeolites. *Applied Catalysis A: General*, 306, 78–84. DOI: 10.1016/j.apcata.2006.03.030.

[39] Khairina, N.N.L., Kristiani, A., Widjaya, R.R., Agustian, E., Dwiatmoko, A.A. (2022). Conversion of fatty acid into biodiesel using solid catalysts of Ti-Zr and Ti-Cr pillared bentonite. *AIP Conf. Proc.* 2493, 060017. DOI: 10.1063/5.0110942.

[40] Machfud, M., & Rusmini, R. (2017). Pengaruh Waktu Interaksi Bentonit Teraktivasi Terhadap Daya Serap Iodium. *Indonesian Chemistry and Application Journal*, 1(1), 10. DOI: 10.26740/icaj.v1n1.p10-17.

[41] Siregar, S.H., & Irma, W. (2016). Sintesis Dan Perbandingan Struktur, Tekstur Bentonit Alam Dan Bentonit Teraktivasi Asam. *Photon: Jurnal Sain Dan Kesehatan*, 7(01), 137–140. DOI: 10.37859/jp.v7i01.572.

[42] Agustian, E., Juwono, A.L., Rinaldi, N., Dwiatmoko, A.A. (2023). Pillaring of bentonite clay with Zr, Ti, and Ti/Zr by ultrasonic technique for biodiesel production. *South African Journal of Chemical Engineering*, 45, 137–140. DOI: 10.1016/j.sajce.2023.06.001.

[43] Wang, G., Hua, Y., Su, X., Komarneni, S., Ma, S., Wang, Y. (2016). Cr(VI) adsorption by montmorillonite nanocomposites. *Applied Clay Science*, 124–125, 111–118. DOI: 10.1016/j.clay.2016.02.008.

[44] Ruslan, Khairuddin, Hardi, J., Mirzan, M. (2020). Characterization of zirconia-pillared clay with sulfate acid activation. *AIP Conf. Proc.* 2243, 030022. DOI: 10.1063/5.0001508.

[45] Binitha, N.N., Sugunan, S. (2006). Preparation, characterization and catalytic activity of titania pillared montmorillonite clays. *Microporous and Mesoporous Materials*, 93(1–3), 82–89. DOI: 10.1016/j.micromeso.2006.02.005.

[46] Fatimah, I., Narsito, N., Wijaya, K. (2011). Effect of Aluminium Content in Aluminium Pillared Montmorillonite on Its Surface Acidity Properties. *ITB Journal of Sciences*, 43(2), 123–138. DOI: 10.5614/itbj.sci.2011.43.2.5.

[47] Sun, J., Wang, Y. (2014). Recent advances in catalytic conversion of ethanol to chemicals. In *ACS Catalysis* 4 (4), 1078–1090. DOI: 10.1021/cs4011343.

[48] Fayisa, B.A., Xi, Y., Yang, Y., Gao, Y., Li, A., Wang, M.-Y., Lv, J., Huang, S., Wang, Y., Ma, X. (2022). Pt-Modulated Cu/SiO2 Catalysts for Efficient Hydrogenation of CO2-Derived Ethylene Carbonate to Methanol and Ethylene Glycol. *Chin. J. Chem. Eng.*, 41, 366–373. DOI: 10.1016/j.cjche.2021.10.024.

[49] Anwar, M.S., Widjaya, R.R., Prasetya, L.B.A., Arfi, A.A., Mabruri, E. (2022). Effect of Grain Size on Mechanical and Creep Rupture Properties of 253 MA Austenitic Stainless Steel. *Metals*, 12(5), 820. DOI: 10.3390/met12050820.

[50] Widjaya, R.R., Juwono, A.L., Rinaldi, N. (2017). Bentonite modification with pillarization method using metal stannum. *AIP Conf. Proc.* 1904, 020010. DOI: 10.1063/1.5011867.

[51] Virkutye J., Varma R.S. (2014). Eco-friendly magnetic iron oxide-pillared montmorillonite for advanced catalytic degradation of dichlorophenol. *ACS Sustain. Chem. Eng.* 2, 1545–1550. DOI: 10.1021/sc5002512.